Scientific Research Publishing

Materials Sciences and Applications, 2022, 13, 342-357
https://www.scirp.org/journal/msa
ISSN Online: 2153-1188
ISSN Print: 2153-117X

Effects of Vanadium on Structure and Tensile Properties of Tempcore Steel Bars

Hany Khalifa*, A. El-Kady

EZZ Steel, Cairo, Egypt
Email: *hany-khalifa@ezzsteel.com

How to cite this paper: Khalifa, H. and El-Kady, A. (2022) Effects of Vanadium on Structure and Tensile Properties of Tempcore Steel Bars. *Materials Sciences and Applications*, **13**, 342-357.
https://doi.org/10.4236/msa.2022.135019

Received: February 20, 2022
Accepted: May 28, 2022
Published: May 31, 2022

Abstract

Thermomechanical processing is a metallurgical operation to produce high-strength steel bars (rebars), through combining plastic deformation with thermal processes like heat treatment, water quenching, heating, and cooling at various rates into a single process. Ribbed reinforcing steel bars (rebars) are used for the reinforcement of concrete structures. Tempcore is a unique process to produce high-yield-strength rebars from mild steel without addition of a high weight percentage of costly alloying elements. The strength of rebar originates from the formation of a surface layer consisting of quenched and tempered martensite that surrounds a core composed of ferrite and pearlite. The economic advantages of this process are significant in comparison to those processes requiring alloying elements or further metal working to improve the mechanical properties. However, when there is a limitation in the water-cooling capacity, the required volume fraction of the martensite layer can't be accomplished particularly when rolling bigger diameters of 32 mm - 40 mm at a higher rolling speed to maintain high productivity. Accordingly, a small addition of microalloying elements vanadium or niobium could be used in combination with Tempcore process to obtain high-strength steel rebars. In this contribution, 0.06 weight percentage of vanadium is added to the Tempcore treated rebars to satisfy ASTM A 706 Standard of Rebar Grade 80 PSI [550 MPa]. In order to decrease the trials in the steel plant floor, thermodynamics equilibrium calculations are predicted by Thermo-Calc, CCT, TTT diagrams are calculated by JMat Pro and the kinetics evolution of the vanadium carbonitrides precipitates are predicted by the computational database Mat Calc. High yield strength and tensile strength are obtained due to the effect of fine dispersions of nanometer-scale vanadium carbonitrides precipitates inspected by transmission electron microscope.

Keywords

Tempcore, Micro-Alloyed Steel, Precipitation Hardening, Thermodynamics of Equilibrium, Kinetics of Formation

1. Introduction

Reinforcing rebars are cylindrical steel bars used for the reinforcement of concrete structures with typical diameters varying from 6 to 40 mm [1]. While concrete has excellent properties with regard to loading under compression, steel is a suitable material to bear high tensile loads. The advantage of the composite structure is the ability to absorb both high compressive and high tensile loads. Rebars are made from medium-carbon steels with a carbon content of approx 0.3 wt% [2] [3]. Actual methods for the production of high-strength concrete reinforcing steels may be classified into three distinct categories:

- The first one consists of steel bars slowly cooled in the air after hot rolling (hot-rolled steels). For these steels, modifying their chemical composition can increase the yield strength, however, for sake of weldability, the carbon and manganese levels should be kept low and this necessarily results in low strength.
- Secondly, small additions of strong carbide formers, such as Nb or V, may enhance the yield strength without affecting weldability. But it is rather expensive.
- The third category consists of bars submitted to specific thermomechanical strengthening processes, bearing trade-name Tempcore [1] [2] [3] [4].

1.1. Principle of the Tempcore Process

Tempcore is one of the thermomechanical processes developed by CRM. A typical manufacturing route is the so-called Tempcore process. The Tempcore installation is in-line connected to the hot rolling mill, directly after the finishing stand and consists of three stages as follows [1] [2]:

- The rebar leaving the last stand of the hot rolling mill passes through a special water-cooling section. The cooling efficiency of this installation is such that a surface layer of the bar is quenched into martensite, the core remaining austenite. The quenching treatment is stopped when a determined thickness of martensite has been formed under the skin (outer part of the bar section dropping below the martensite transformation starting temperature (Ms).
- When the rebar leaves the intense cooling section, the temperature gradient established in its cross section causes heat to release from the center to the surface. This increase in the surface layer temperature results in the self-tempering of the martensite. The name TEMPCORE has been chosen to illustrate the fact that the martensitic layer is tempered by the heat left in the CORE at the end of the quenching stage.

- Finally, during the slow cooling of the rebar on the cooling bed, the austenitic core transforms into ferrite and perlite or into bainite.

The three stages of the Tempcore process clearly appear:

1) Quenching of the surface layer;

2) Self-tempering of the martensite;

3) Transformation of the core.

The tempcore process has become a very popular solution for producing high-strength and weldable reinforcing concrete bars (rebars) from low C/Mn steel without requiring the costly addition of V or Nb for most of the grades to produce. However, the water quenching and self-tempering treatment should be applied without any reduction of rolling speed or loss of productivity. Producing big sizes and high-strength steel grades could be confronted with the mill layout and mill constraints, leading to rolling speed reduction [5] [6] [7].

By a sensible combination of Tempcore treatment and microalloying chemistry (Precipitation hardening,) higher grades can be realized, especially for large diameters of 32 - 40 mm.

1.2. Principle of Precipitation Hardening

Precipitation hardening represents one of the most efficient ways to improve the mechanical properties of metallic alloys and thus receives continuous close attention in metallurgy and kinetics of the formation of the carob-nitrides precipitates. Nanometer-scale precipitates account for the strength of ferrite/pearlite steel without impeding ductility and formability [8]-[14]. The nucleation and growth of such nanometer-scale precipitates are enabled by microalloying elements such as Ti, Nb and V during steelmaking. The abundance of carbon and nitrogen in ferrite results in the formation of carbonitrides, such as titanium carbonitrides (TiCN), niobium carbonitrides (NbCN) and vanadium carbonitrides (VCN) [15] [16] [17] [18] [19]. The strength of microalloyed steel relies on small particle size (nanometer-scale) and a high number density of precipitates [20] [21] [22] [23]. Therefore, adjusting and maintaining the fine precipitate size during steel processing and elevated temperature service is crucial to achieve and keep strength in the final component [20] [21] [22] [23] [24].

In this context, the current work aims to develop steel alloys with tailored chemical composition and thermomechanical controlled processing TMCR schedule to produce high-strength reinforcing bars ASTM A706 grade 80 (55). [17].

2. Methodology Thermodynamic Calculations and Experimental Work

The alloy is first melted and the chemical composition is adjusted in the electrical arc furnace EAF and ladle furnace LF. The melted steel is cast in the form of billets. These billets are further thermomechanical processed in the rolling mill plant equipped with a reheating furnace, mill train, quenching box and cooling

bed. In the current work, thermodynamic and kinetics calculations were performed prior to the production process. Therefore, tailored alloy and thermomechanical schedule adequate to the lay-out arrangement and capacity constraints of the industrial plant are developed. A number of calculations of phase equilibrium diagrams with numerous alternative compositions considering maximum carbon weight percentage of 0.3%, different silicon Si, Mn and V weight percentage were plotted by Thermo-Calc software. For each proposed composition the corresponding continuous cooling transformation CCT diagram and precipitation volume fraction diagrams were predicted by the kinetics computational programs JMat pro and MatClac. From these calculations the composition of the alloy in the current study is selected. Table 1 presented the designed alloy along with the requirements defined in ASTM A 706 [17] with the exception of Vanadium because it is an important addition for the purpose of getting precipitation hardening.

To verify that the selected alloys enables sufficient vanadium, nitrogen and carbon enrichment for precipitates formation during the cooling route, TECF 10 data base was used for thermodynamic calculations to predict the amount of phases, the Equilibrium amount of FCC_A1#2 V(C, N), enrichment of V(C, N) with alloying elements vanadium, carbon and nitrogen while the temperature is decreasing.

The most important parameter in controlling the mechanical properties of microalloyed steel is the reheating temperature, which affects the solid solute V content and austenite grain size. Therefore, thermodynamic calculations are also used to determine the reheating temperature of the billets. In this content, reheating temperature of micro alloyed steel should be sufficiently high to confirm the dissolution of vanadium carbide and nitride precipitates.

Kinetics of precipitations is also predicted to ensure enough kinetics for the formation of vanadium precipitation during cooling schedule.

CCT and TTT diagrams are plotted by JMat Pro software to define the formed phases during the entire thermomechanical treatment cycle.

2.1. Thermomechanical Controlled Rolling TMCR

The tested alloy was subjected to the thermomechanical schedule designated in Figure 1. In this schedule, billets were austenitizing at reheating furnace. According to the thermodynamic calculations, billet reheating values of 1050˚C is selected to dissolve the V(C, N). To achieve improved combination of strength and ductility a significant amount of deformation occurs in the lower austenite region. The austenite is deformed in a temperature of 1050˚C - 1000˚C in order to refine the austenite grain size.

Table 1. ASTM A706 [17] and the considered alloy.

Element	C, Wt%	Si, Wt%	Mn, Wt%	V, Wt%	P, Wt%	S, Wt%	N, PPM
ASTM 706 (Max.)	0.3	0.5	1.5	N/A	0.035	0.045	N/A
The tested Alloy	0.26	0.3	1.5	0.06	0.025	0.03	110

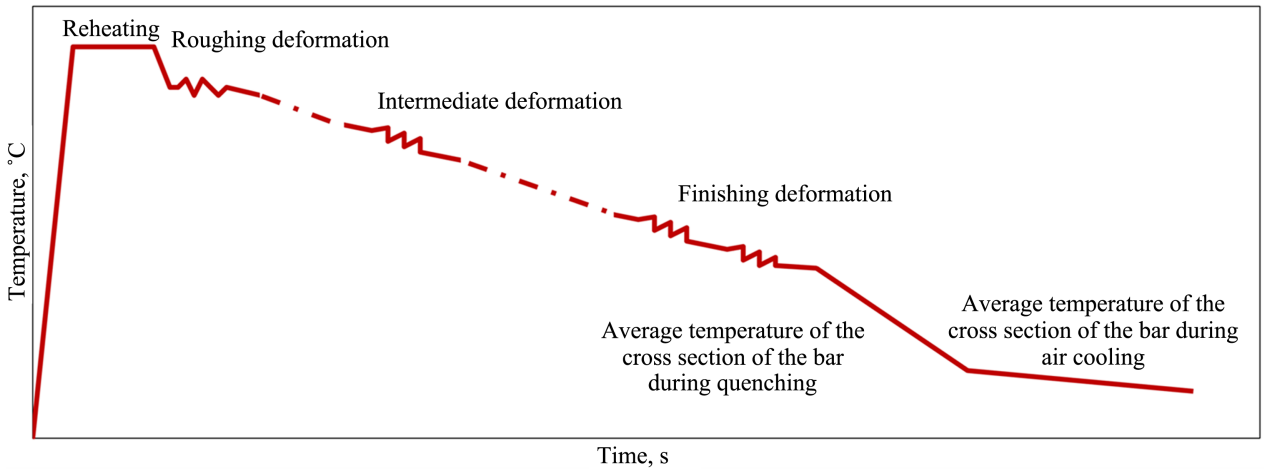

Figure 1. Thermomechanical schedule.

An intense water cooling is applied to the whole surface of the rebar for 1.5 to 2 seconds directly after the last rolling pass. Cooling is interrupted before the core is affected by quenching and the outer layers are tempered by the flow of heat from the core to the surface. At the exit of the finishing stand directly temperatures are typically at 980˚C. After cooling over the whole surface of the section a self-tempering temperature if 580˚C - 620˚C. **Figure 2** shows the thermal gradient of the Tempcore treated bar starting from the entry of quenching box till equalizing between core and surface takes place at cooling bed (developed in other work by H. Khalifa *et al.*) [25].

Reheating, rolling and tempering temperatures were measured by in-line pyrometers. The pyrometers are the heart of the control of the process. The location of the tempering pyrometer is of prime importance to get measurements as close as possible to the maximum recovery temperature (maximum reached by the surface). The pyrometer located at the entry of the Tempcore box is also important to measure the variation of finishing temperature along the billet or between successive billets. The location of the reheating furnace pyrometer is very important to confirm that the undesired vanadium carbonitrides inside the billets are completely dissolved.

The cooling length and quenching time are linked by the rolling speed at the finishing stand. This speed is maintained constant along the billet during its crossing of the quenching equipment, and more particularly when the tail of the billet is leaving the finishing stand. This is controlled by the pinch-roll located between the exit of the Tempcore box and the dividing shear. Without using this pinch-roll, when the tail leaves the finishing stand, small rebar diameters are braked by the water while the largest diameters are accelerated.

2.2. Microscopy

2.2.1. Light and Scanning Electron Microscopies

Light optical microscopy (LOM) and scanning electron microscopy (SEM) of the samples after applying various processing conditions were performed on

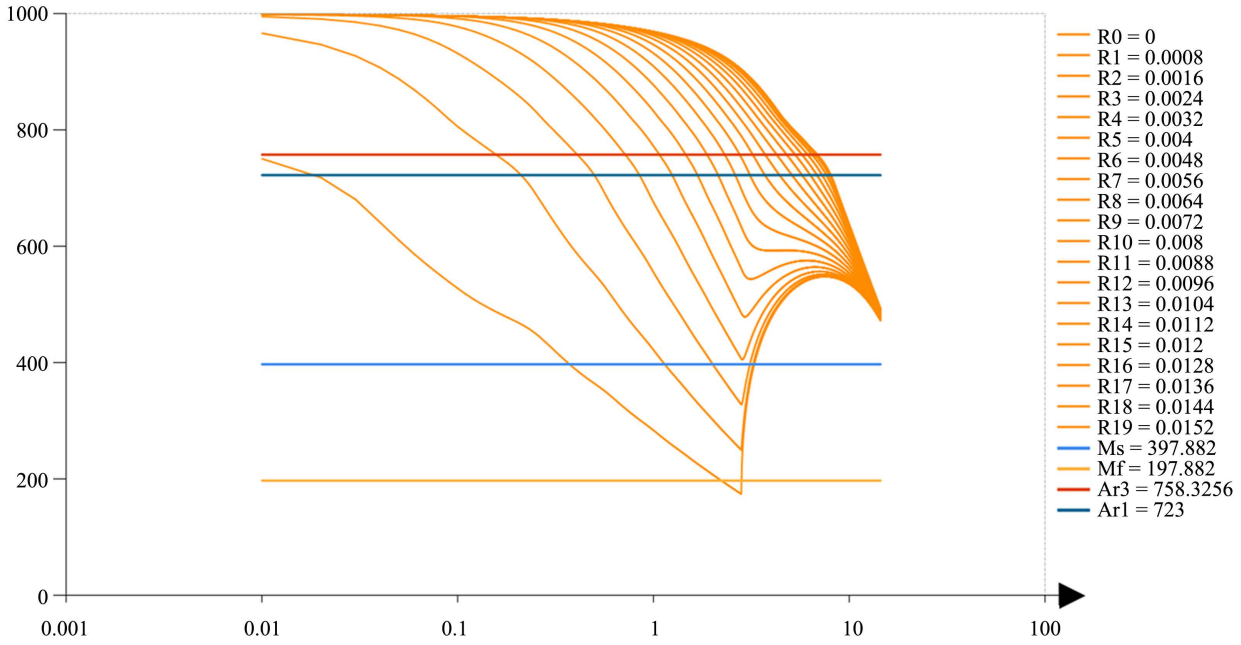

Figure 2. Thermal history of the cross section of the bar during water quenching and air cooling at cooling.

sections cut at the cross section of the entire diameter of the specimens. The specimens were mounted and subsequently prepared by standard mechanical grinding and polishing methods. The investigated samples were ground gradually using wet silicon carbide papers preliminary with 180-grit, followed by 240-, 400-, 500-, 600-, 800-, 1000- and 1200-grit papers consequently. Final polishing was done using 1.0 μm and 0.05 μm alumina, respectively. The microstructure of the specimens was revealed by 0.5% nital etchant alcohol. The ferrite grain size was measured by applying the mean linear intercept method according to ASTM E112-13 [26].

2.2.2. Scanning Transmission Electron Microscopy (STEM) Examinations

Scanning transmission electron microscopy (STEM) is used for studying vanadium precipitates morphology and size distribution since it is the most widely used technique to test phases over the length scale range 1 - 100 nm. A high energy electron beam (typically 200 kV) is focused on the thin foil sample parallel to the optic axis of the microscope with a beam diameter of 1 - 25 mm. The transmitted beam undergoes coherent elastic ('Bragg') diffraction. Carbon replicas of the sample were made for further investigation of the precipitates by means of scanning transmission electron microscopy (STEM). Energy Dispersive X-Ray Spectroscopy (EDX) in a carbon replica of the sample is investigated to recognize the type of the precipitates.

2.3. Tensile Test

Yield strength, ultimate tensile strength, and elongation of the investigated bars were estimated at room temperature by universal tensile testing machine with a cross-head speed of 0.1 mm/s according to the (ASTM E8/E8M-16ae1) [27].

2.4. Hardness Test

Microhardness tester was used to measure the Vickers hardness of the samples. The sample surfaces were ground using a similar method described in the micrograph preparation up to the 1200 grit sandpaper. Measurements were taken using a load of 2.9 N applied for 10 seconds. The micrometers (both X and Y axis) attached to the sample table of the tester were used to determine the center of the samples and to increment the sample between readings. In this way measurements were taken at equal increments along the radius of the sample. In addition, as illustrated in Figure 3, measurements along two radii 90 degrees apart were taken and then averaged.

3. Results and Discussion

3.1. Thermodynamic Calculations

The equilibrium development of phases and precipitates were examined using TCFE10 database of Thermo-Calc software. The relationship between the amounts of phases corresponding to the temperature ranging from 500˚C to 1000˚C is plotted as presented in Figure 4(a) the graphs prove that vanadium carbonitrides has high solubility level in austenite, this allows using lower reheating and soaking temperature as 1000˚C. Observably, the tested alloy shows the formation of V(C, N) phase below 1000˚C stating that the start of the formation of the precipitation of V(C, N) particles starts at the austenite grain boundaries and extends into ferrite phase. Therefore, reheating of the billet at 1050˚C achieves full dissolution of vanadium carbonitrides to be available for later precipitation during the consequent rolling and cooling process. The formation of ferrite start temperature of 800˚C, while the cementite formations starts at the temperature below 700˚C, where the austenite phase is no longer exists and completely decomposes. To further clarify the amount of free nitrogen, vanadium and carbon which is ready for the formation of vanadium carbonitrides, the values of %V, %C and %N in solution in austenite is plotted as illustrated in Figure 4(b). The equilibrium carbonitrides composition and its volume fraction were also calculated as presented in Figure 4(c), the figures clearly show that, the precipitate has a significant amount of nitrogen. This can be seen not only in Figure 4(b) but also in Figure 4(c).

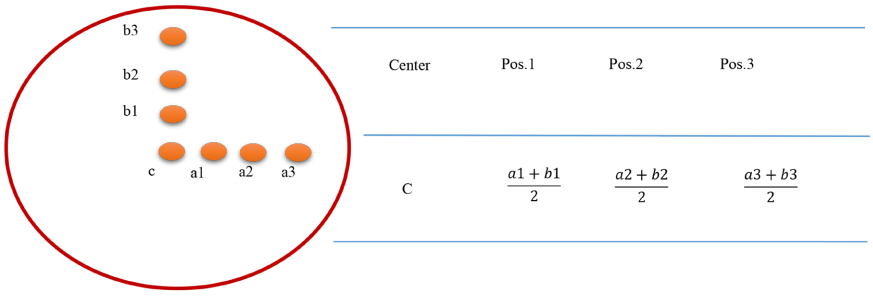

Figure 3. Micro-hardness measurement arrangement.

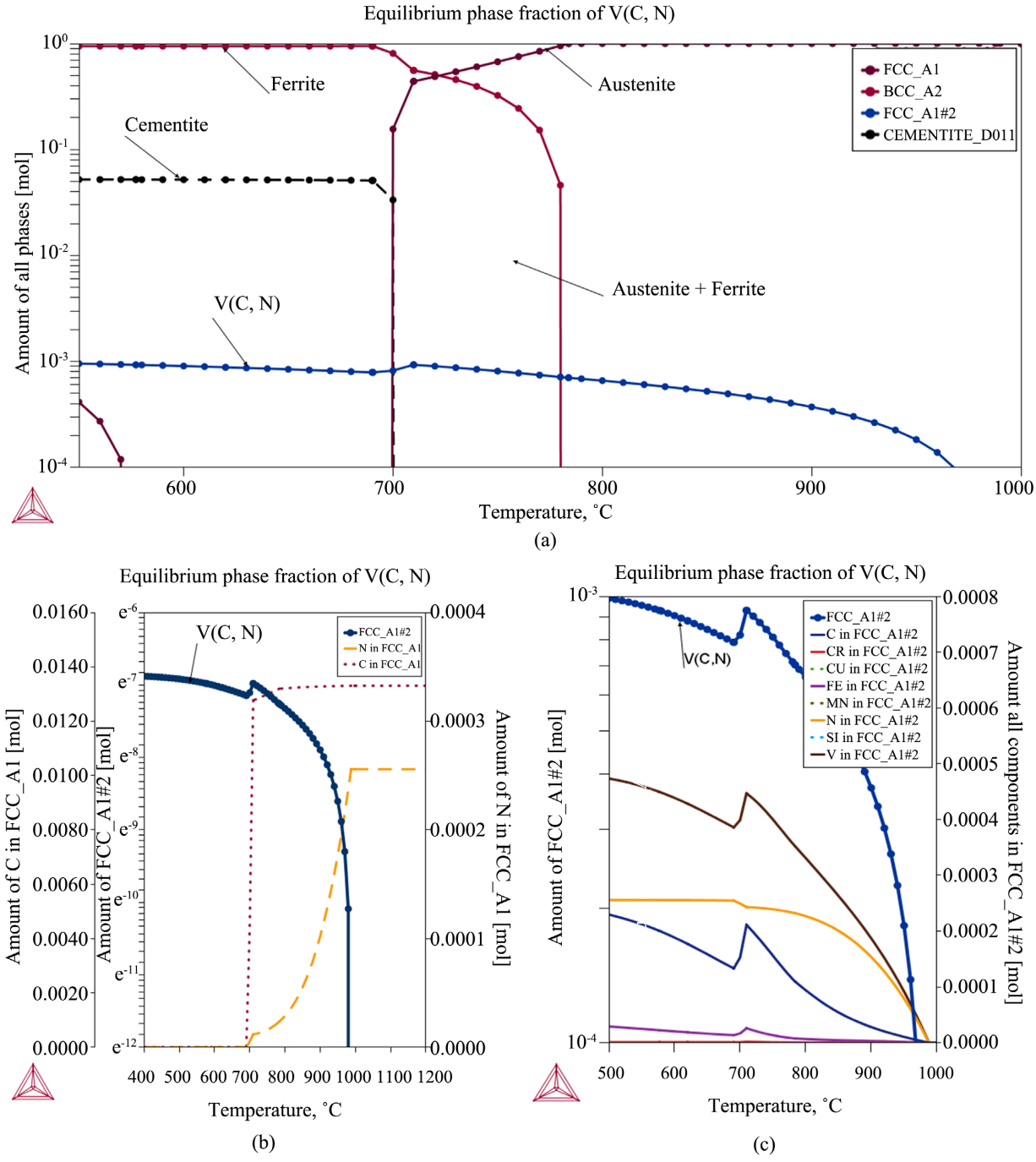

Figure 4. (a)-(c): (a) Formation of phases in the investigated steel, (b) The Equilibrium amount of FCC_A1#2 (V(C, N), amount of nitrogen and carbon in austenite, (c) enrichment of V(C, N) with alloying elements vanadium, carbon and nitrogen while the temperature is decreasing.

3.2. CCT and TTT Diagrams

Continuous cooling transformations (CCT) diagram and time temperature transformation (TTT) diagram of the investigated steel were predicted by JMat-Pro, Sente software as shown in **Figure 5**. TTT and the CCT curves indicate that the ferrite transformation start temperature is 780˚C and the incubation time

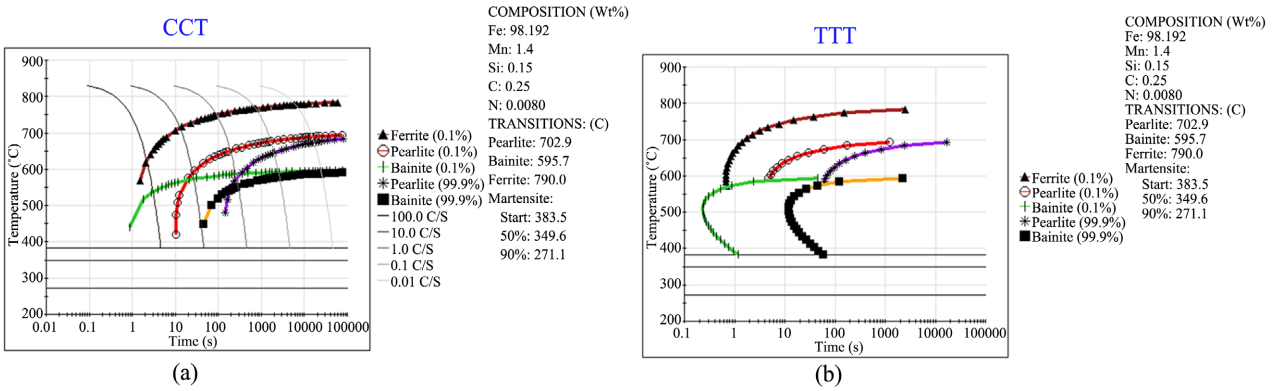

Figure 5. (a) CCT diagram, (b) TTT diagram.

required for the onset of ferrite transformation is 100 S at high temperature transformation of 780˚C, while the incubation time required for the onset of ferrite transformation decreased to 5 - 10 s in the lower ferrite transformation temperature range from 600˚C to 700˚C due to the increase in the driving force of transformation. This relatively high incubation time is a clear indication that the addition of 0.06 Wt% vanadium increases the hardenability of the tested steel. It is evident from CCT curve that water cooling rate more than 100˚C/S is high enough to avoid the formation of ferrite, pearlite and bainite, therefore hard martensite phase is formed in the surface layer of the bar. As the cooling rate in the core decreases, therefore martensite will not be formed and ferrite-pearlite microstructure is formed with chances of bainite intermediate zone.

3.3. Kinetics of V(C, N) Precipitates

The nature, size and distribution of V-containing carbide, nitride or carbo-nitride precipitates depend not only on the V content but also on the thermomechanical cycle. Therefore, the kinetics of V(C, N) of the cooling schedule is simulated based on the thermal profiles calculated by the model developed by Khalifa *et al.* [25] depicted in **Figure 2**. Thermal profiles for the outer surface as well as for the core of the tested diameter (32 mm) is set as the heat-treatment cycles for precipitations kinetics simulations. The relation between the resulting phases fractions of precipitates versus time in seconds are predicted as presented in **Figure 6**.

The kinetics simulation indicates a variation in precipitation potential depending on the layers of the cross section. Obviously, the core evident a greater potential to form higher volume fractions of V(C, N) precipitates compared with the outer surface.

The fractions of V(C, N) precipitates reach approximately 0.0006 for outer surface and 0.0014 for the core. The lower fractions of V(C, N) precipitates in the surface could be attributed to the fact that the precipitation kinetics generally shows a sluggish behavior as the temperature dropped rapidly. Contradictory, the higher volume fractions of V(C, N) precipitates in the core could be

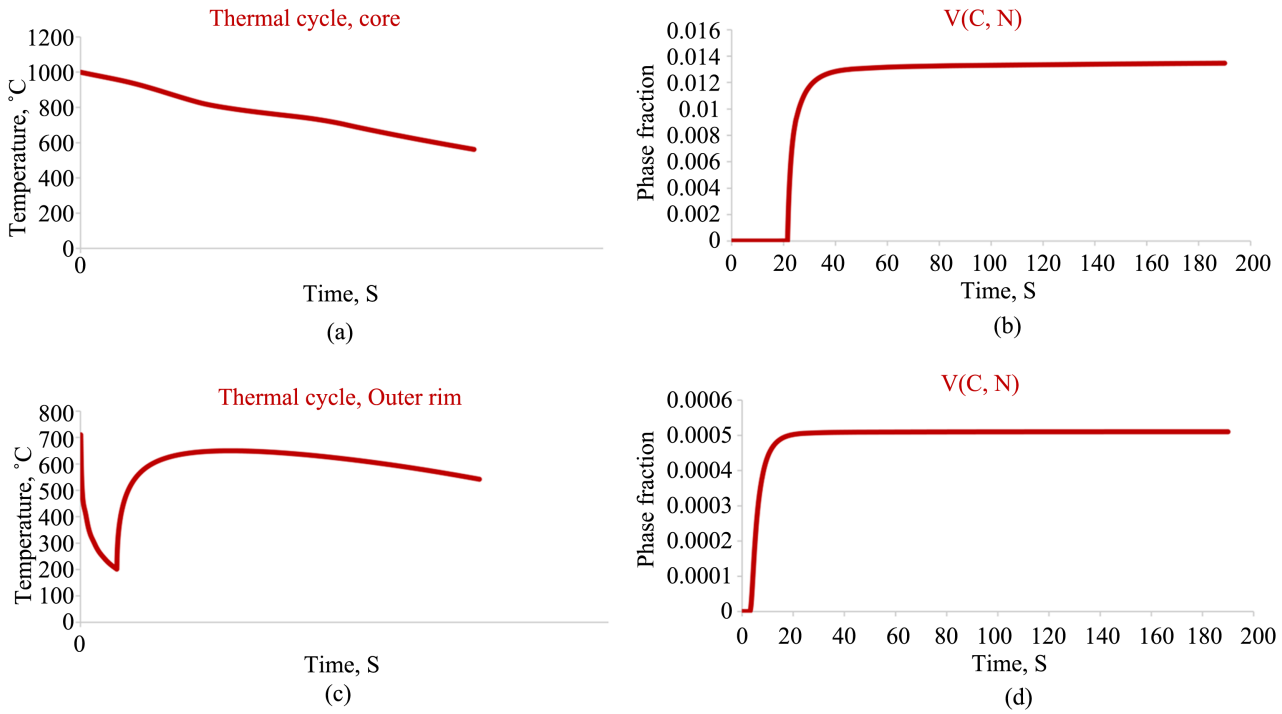

Figure 6. Phase fraction of vanadium precipitates corresponding to the core and the outer surface.

attributed to the larger time-window available for precipitation kinetics as the cooling rate is very slow and the temperature is high (tempering temperature is 580˚C - 620˚C).

3.4. Microstructure Characteristics

3.4.1. Light Optical Microscope

Microstructure was examined under an optical microscope. Micrographs were captured with a digital camera connected to the microscope. The macro structure is presented in **Figure 7(a)**, whereas the microstructure in the cross-section is presented in **Figure 7(b)**, **Figure 7(c)** and **Figure 7(d)**, it consists of three main zones: a fine ferrite-pearlite core (**Figure 7(b)**), an intermediate hardened layer with a mixture of bainite and ferrite (**Figure 7(c)**) and a tempered martensite-hardened layer on the surface (**Figure 7(d)**). Relatively larger amounts of pearlite are observed due to the effect of the Tempcore process. The volume percentages of martensite, bainite and pearlite phases were obtained from etched specimens as 25%, 5% and 70% respectively. The addition of V doesn't significantly affect the ferrite grain size, since it reduces ferrite grain size from 6 to 5μm.

3.4.2. Scanning Electron Microscope SEM

The microstructures of the specimen tested by Scanning electron microscope SEM is presented in **Figure 8(a)** and **Figure 8(b)**. The outer rim zone for the Tempcore treated alloy **Figure 8(a)** shows tempered martensite with lath like morphology consisting of differently oriented martensite packets containing

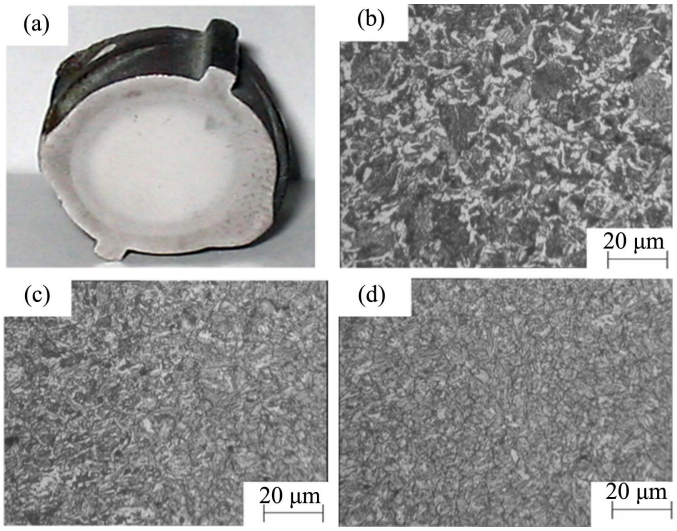

Figure 7. (a) Microstructural variation in a cross-section of a Tempcore reinforcing steel bar, (b) ferrite-pearlite core, (c) mixture of bainite and ferrite and (d) tempered martensite hardened-layer.

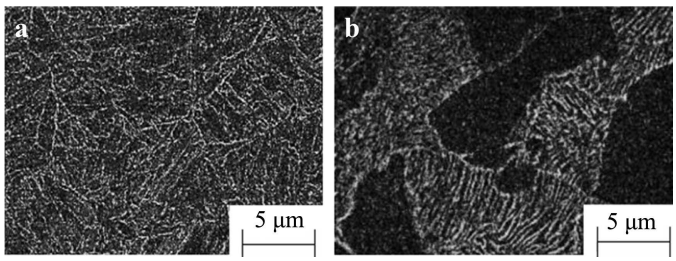

Figure 8. SEM micrographs of the tested alloys. (a) Tempered martensite in the surface, (b) ferrite-pearlite microstructures in the core.

various blocks of martensite lathes indicate the possible carbonitrides precipitates during the Tempcore process. The microstructures of the core zone of Tempcore treated bar Figure 8(b) consists of ferrite-pearlite structure with typical lamella structure of pearlite.

3.4.3. Transmission Electron Microscope TEM

TEM micrograph presented in Figure 9(a) shows a fine precipitation of V(C, N) within the ferrite grains and on the grain boundaries. The precipitates are distributed in the grain boundaries and often occur in straight lines, indicating nucleation on a moving austenite/ferrite boundary. The precipitation of V(C, N) within the ferrite grains are found to be distributed in a random fashion.

TEM micrographs are explained by thermodynamics and kinetics calculations, since the fine V(C, N) precipitates primarily form during and after the austenite to ferrite transformation. Since the core is cooled down at a slow-rate until the equalizing temperature ranging from 580˚C to 620˚C. In the quenched rim on the surface it is expected that lower volume fraction of V(C, N) due to the less time-window available for the kinetics of formation. Figure 9(b) shows fine particles revealed by means of Energy Dispersive X-Ray Spectroscopy

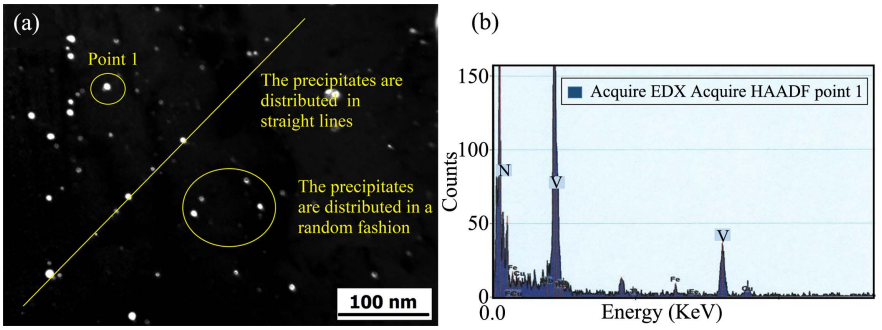

Figure 9. (a): the precipitates investigated by means of STEM of its carbon replica, (b): EDX analysis at point 1 which marked with circle.

(EDX) in a carbon replica of the sample with the microstructure shown in **Figure 9(a)**: The EDX analysis gives a hint that the precipitates either VN or V(C, N) or either mixture. As the sample is carbon replica, it cannot be clearly identified in which form they are.

3.5. Hardness Vickers Profile

Figure 10 shows typical microhardness curves measured for the tested bar. It is observed that the hardness variation is continuous from the surface to the center. The surface hardness decreases as a result of an increase in tempering temperature of martensite and the core hardness decreases as a result of an increase in transformation temperature. Hardness profile exhibits a slight decrease near the surface of the bar; this is attributed to surface decarburization of the surface of the billets in the reheating furnace.

3.6. Tensile Properties

Stress - strain curves of the TMCP steel bars are presented in **Figure 11**. The stress–strain curves shows enhanced tensile properties as expected from the fine and homogenous distribution of vanadium precipitates as appeared in the microstructure characterization of the tested steel. A pronounced effect of the proper alloy design and thermomechanical processing on mechanical properties is obvious. The effect of vanadium precipitates is contributing in the highest level of ultimate tensile (U.T.S) and yield strength (Y.S) with a good values of total elongation (TEl), with U.T.S = 785 MPa, Y.S = 580 MPa and TEl = 18%.

The increase in strength is also achieved due to the contribution of nitrogen since higher nitrogen contents decreases the inter-particle spacing. The greatest strengthening effect from vanadium precipitation occurs when inter-particle spacing is minimized, resulting in more instances of the Orowan bowing strengthening mechanism. Higher nitrogen contents decrease inter-particle spacing by increasing the driving force for VN nucleation, resulting in increased precipitation strengthening at higher nitrogen contents [28].

Carbon content also has a significant effect on vanadium precipitation and precipitation strengthening. The mechanism by which carbon aids in precipitation strengthening is different from nitrogen. The high solubility of VC and

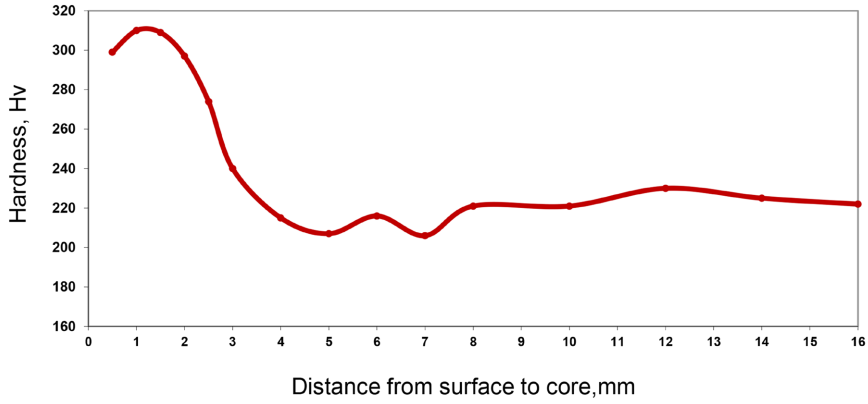

Figure 10. Hardness distribution for tested reinforcing bars versus normalized radius of bar.

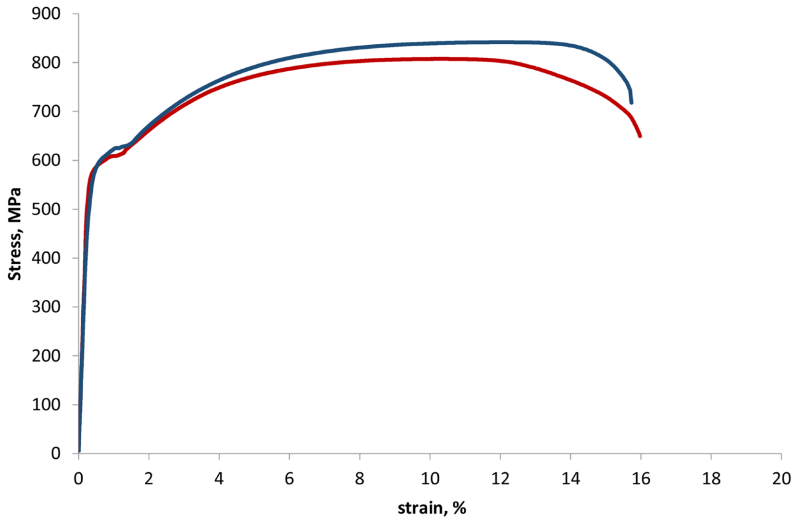

Figure 11. Stress-strain curves for the base alloy and three TMCR samples.

lower driving force for nucleation However, carbon helps to stabilize austenite to a lower γ/α transformation temperature. Stabilizing austenite to lower temperatures delays the vanadium solubility drop that occurs during the γ/α transformation, resulting in finer VN and V(C, N) precipitation [29].

4. Conclusions

1) In this study, tailored composition with microalloying element V along with a thermomechanical schedule is applied to produce rebars with a diameter of 32 mm satisfying the requirements of ASTM A706.

2) The steel reported in the current work exhibits yield strength as high as 580 MPa and tensile strength as high as 750 MPa. An increase in the strength is the result of the facilitated precipitation in the ferrite and at the prior austenite grain boundaries. The precipitates form a sufficient hard phase to enhancethe strength.

3) The precipitates formed in the ferrite due to the slow cooling rates in the

core of the Tempcore treated bars. Since, lower cooling rates at the core of the rebar permit the kinetics of the formation of V(C, N) with high precipitation volume fraction.

4) It appears that vanadium has no effect on grain size and that the increase in strength is due primarily to the precipitation of vanadium carbides and nitrides.

Conflicts of Interest

The authors declare no conflicts of interest regarding the publication of this paper.

References

[1] Park, C.S., Yi, H.J., Kim, Y.-T., Han, S., Lee, T. and Moon, Y.H. (2019) Tempcore Process Simulator to Analyze Microstructural Evolution of Quenched and Tempered Rebar. *Applied Sciences*, **9**, 2938. https://doi.org/10.3390/app9142938

[2] Nikolaou, J. and Papadimitriou, G. (2004) Microstructures and Mechanical Properties after Heating of Reinforcing 500 MPa Class Weldable Steels Produced by Various Processes (Tempcore, Microalloyed with Vanadium and Work-Hardened). *Construction and Building Materials*, **18**, 243-254. https://doi.org/10.1016/j.conbuildmat.2004.01.001

[3] DiMatteo, A., Vannucci, M. and Colla, V. (2015) A Finite Element Method for the Prediction of Thermal, Metallurgical, and Mechanical Behavior of Rebars in the TempCore Process. *Steel Research International*, **87**, 276-287. https://doi.org/10.1002/srin.201500029

[4] Sankar, I.B., Rao, K.M. and Krishna, A.G. (2009) Prediction of Heat Transfer Coefficient of Steel Bars Subjected to Tempcore Process Using Nonlinear Modeling. *The International Journal of Advanced Manufacturing Technology*, **47**, 1159-1166. https://doi.org/10.1007/s00170-009-2240-3

[5] Bandyopadhyay, K., Lee, J., Shim, J.-H., Hwang, B. and Lee, M.-G. (2019) Modeling and Experiment on Microstructure Evolutions and Mechanical Properties in Grade 600 MPa Reinforcing Steel Rebar Subjected to TempCore Process. *Materials Science and Engineering*: *A*, **745**, 39-52. https://doi.org/10.1016/j.msea.2018.12.079

[6] Khalifa, H., Megahed, G., El-Bitar, T. and Taha, M. (2020) Development of Direct Hot-Rolled Ultralow-Carbon Pre-Peritectic Ferrite-Bainite Dual-Phase Steel for a Compact Slab Production Plant. *Journal of Materials Engineering and Performance*, **30**, 5773-5786. https://doi.org/10.1007/s11665-021-05789-y

[7] Khalifa, H., Megahed, G., El-Bitar, T. and Taha, M. (2020) Development of Tailored Structure and Tensile Properties of Thermomechanical Treated Micro Alloyed Low Carbon Dual Phase Steel. *Materials Sciences and Applications*, **11**, 851-866. https://doi.org/10.4236/msa.2020.1112056

[8] Wen, H., Topping, T.D., Isheim, D., Seidman, D.N. and Lavernia, E.J. (2013) Strengthening Mechanisms in a High-Strength Bulk Nanostructured Cu-Zn-Al Alloy Processed via Cryomilling and Spark Plasma Sintering. *Acta Materialia*, **61**, 2769-2782. https://doi.org/10.1016/j.actamat.2012.09.036

[9] Liu, J., Yu, H., Zhou, T., Song, C. and Zhang, K. (2014) Effect of Double Quenching and Tempering Heat Treatment on the Microstructure and Mechanical Properties of a Novel 5Cr Steel Processed by Electro-Slag Casting. *Materials Science and Engineering*: *A*, **619**, 212-220. https://doi.org/10.1016/j.msea.2014.09.063

[10] Bikmukhametov, I., Beladi, H., Wang, J., Hodgson, P.D. and Timokhina, I. (2019)

The Effect of Strain on Interphase Precipitation Characteristics in a Ti-Mo Steel. *Acta Materialia*, **170**, 75. https://doi.org/10.1016/j.actamat.2019.03.022

[11] Khalifa, H., Megahed, G.M., El-Bitar, T. and Taha, M.A. (2020) Development of Tailored Structure and Tensile Properties of Thermomechanical Treated Micro Alloyed Low Carbon Dual Phase Steel. *Materials Sciences and Applications*, **11**, 851-866. https://doi.org/10.4236/msa.2020.1112056

[12] Zhou, T., Babu, R.P., Odqvist, J., Yu, H. and Hedström, P. (2018) Quantitative Electron Microscopy and Physically Based Modelling of Cu Precipitation in Precipitation-Hardening Martensitic Stainless Steel 15-5 PH. *Materials & Design*, **143**, 141-149. https://doi.org/10.1016/j.matdes.2018.01.049

[13] Scott, C., Allain, S., Faral, M. and Guelton, N. (2006) The Development of a New Fe-Mn-C Austenitic Steel for Automotive Applications. *Metallurgical Research & Technology*, **103**, 293-302. https://doi.org/10.1051/metal:2006142

[14] Radis, R. and Kozeschnik, E. (2010) Kinetics of AlN Precipitation in Microalloyed Steel. *Modelling and Simulation in Materials Science and Engineering*, **18**, Article ID: 055003. https://doi.org/10.1088/0965-0393/18/5/055003

[15] Miyamoto, G., Hori, R., Poorganji, B. and Furuhara, T. (2011) Interphase Precipitation of VC and Resultant Hardening in V-Added Medium Carbon Steels. *ISIJ International*, **51**, 1733-1739. https://doi.org/10.2355/isijinternational.51.1733

[16] Donga, H., Chen, H., Khorasgani, A., Zhang, B., Zhang, Y., Wang, Z., Zhou, X., Wan, W., Wang, H., Li, T., Yang, Z. and Zwaag, S. (2022) Revealing the Influence of Mo Addition on Interphase Precipitation in Ti-Bearing Low Carbon Steels. *Acta Materialia*, **223**, Article ID: 117475. https://doi.org/10.1016/j.actamat.2021.117475

[17] Maugis, P. and Goune, M. (2005) Kinetics of Vanadium Carbonitride Precipitation in Steel: A Computer Model. *Acta Materialia*, **53**, 3359-3367. https://doi.org/10.1016/j.actamat.2005.03.036

[18] Zhou, J., Hu, C., Hu, F., Hou, T., Yin, C., Zhu, X. and Wu, K. (2022) Insight into the Effect of Nb Microalloying on the Microstructure-Property Relationship of a Novel Wire Rod. *Journal of Materials Research and Technology*, **16**, 276-289. https://doi.org/10.1016/j.jmrt.2021.11.144

[19] Parusov, V.V., Sychkov, A.B., Derevyanchenko, I.V., *et al.* (2004) High-Carbon Wire Rod Made of Steel Microalloyed with Vanadium. *Metallurgist*, **48**, 618-625. https://doi.org/10.1007/s11015-005-0037-7

[20] Yang, Y., Zhang, X.F., Li, Y.M. and Huang, Z.Y. (2020) Isothermal Precipitation Behavior of Vanadium Carbonitride in V-, N-Added Low-Carbon Steel. *Steel Research International*, **91**, Article ID: 2000086. https://doi.org/10.1002/srin.202000086

[21] Bu, F.Z., Wang, X.M., Chen, L., Yang, S.W., Shang, C.J. and Misra, R.D.K. (2015) Influence of Cooling Rate on the Precipitation Behavior in Ti-Nb-Mo Microalloyed Steels during Continuous Cooling and Relationship to Strength. *Materials Characterization*, **102**, 146-155. https://doi.org/10.1016/j.matchar.2015.03.005

[22] Clark, S., Janik, V., Rijkenberg, A. and Sridhar, S. (2016) Analysis of the Extent of Interphase Precipitation in V-HSLA Steels through *In-Situ* Characterization of the γ/α Transformation. *Materials Characterization*, **115**, 83-89. https://doi.org/10.1016/j.matchar.2016.03.021

[23] Chen, C.Y., Yen, H.W., Kao, F.H., Li, W.C., Huang, C.Y., Yang, J.R. and Wang, S.H. (2009) Precipitation Hardening of High-Strength Low-Alloy Steels by Nanometer-Sized Carbides. *Materials Science and Engineering: A*, **499**, 162-166. https://doi.org/10.1016/j.msea.2007.11.110

[24] Zhang, Y.J., Miyamoto, G., Shinbo, K., Furuhara, T., Ohmura, T., Suzuki, T. and Tsuzaki, K. (2015) Effects of Transformation Temperature on VC Interphase Precipitation and Resultant Hardness in Low-Carbon Steels. *Acta Materialia*, **84**, 375-384. https://doi.org/10.1016/j.actamat.2014.10.049

[25] Khalifa, H., Megahed, G., Hamouda, R. and Taha, M. (2016) Experimental Investigation and Simulation of Structure and Tensile Properties of Tempcore Treated Rebar. *Material Processing Technology*, **230**, 244-253. https://doi.org/10.1016/j.jmatprotec.2015.11.023

[26] ASTM E112-13 (2013) Standard Test Methods for Determining Average Grain Size, ASTM International, West Conshohocken. http://www.astm.org/cgi-bin/resolver.cgi?E112

[27] ASTM E8/E8M-16ae1 (2016) Standard Test Methods for Tension Testing of Metallic Materials. ASTM International, West Conshohocken. https://www.astm.org/standards/e8

[28] Seok, M.Y., Choi, I.C., Moon, J., Kim, S., Ramamurty, U. and Jang, J.L. (2014) Estimation of the Hall-Petch Strengthening Coefficient of Steels through Nanoindentation. *Scripta Materialia*, **87**, 49-52. https://doi.org/10.1016/j.scriptamat.2014.05.004

[29] Sonderegger, B. and Kozeschnik, E. (2010) Interfacial Energy of Diffuse Phase Boundaries, in the Generalized Broken-Bond Approach. *Metallurgical and Materials Transactions A*, **41**, 3262-3269. https://doi.org/10.1007/s11661-010-0370-8